Available online at www.sciencedirect.com
SCIENCE DIRECT®
Journal of Nuclear Materials 337–339 (2005) 475–479
journal of nuclear materials
www.elsevier.com/locate/jnucmat

Divertor regimes in NSTX

V.A. Soukhanovskii [a,*], R. Maingi [b], A.L. Roquemore [c], J. Boedo [d], C. Bush [b], R. Kaita [c], H.W. Kugel [c], B.P. LeBlanc [c], S.F. Paul [c], G.D. Porter [a], N.S. Wolf [a], NSTX Research Team

[a] *Lawrence Livermore National Laboratory, Livermore, CA, USA*
[b] *Oak Ridge National Laboratory, Oak Ridge, TN, USA*
[c] *Princeton Plasma Physics Laboratory, Princeton, NJ, USA*
[d] *University of California at San Diego, La Jolla, CA, USA*

Abstract

The identification of divertor operating regimes is of particular importance for heat and particle control optimization in high performance plasmas of a spherical torus, because of the magnetic geometry effects and compactness of the divertor region. Recent measurements of radiated power, heat, and particle fluxes in lower single null and double null NSTX plasmas with 0.8–6 MW NBI heating suggest that the inner divertor is detached at $\bar{n}_e \leqslant 2$–3×10^{19} m^{-3} whereas the outer divertor is always attached. This resilient state exists in most L- and H-mode plasmas. The inner divertor transiently re-attaches in ELMy H-mode plasmas when heat pulses from type I or type III ELMs reach the divertor.

PACS: 52.40.Hf; 52.55.Hc; 52.55.Dy
Keywords: Divertor plasma; Divertor modeling; NSTX; Recycling; UEDGE

1. Introduction

The identification of divertor operating regimes is of particular importance for heat load and particle control optimization in high performance plasmas of a spherical torus (ST). Based on the ability of a divertor to sustain a parallel temperature gradient and effectively dissipate the heat load, three divertor operating regimes have been observed in large aspect ratio tokamaks: a sheath-limited, a high-recycling and a detached regime. Present understanding of the divertor regimes relies on the physics of parallel and perpendicular heat and particle transport, particle drifts, and neutral transport [1], and the studies of the ST geometry implications have just begun [2]. Both the magnetic geometry effects, such as low toroidal field, short connection lengths, large flux expansion ratio, large mirror ratio, and the compactness of the divertor region are the factors which may affect the boundaries of the divertor regimes in the plasma operating space. Progress toward an L-mode plasma regime with a detached divertor has been made in the MAST spherical tokamak [3]. Observations of the sheath-limited and high-recycling regimes and the simultaneous inner and outer divertor detachment in a balanced double null configuration have been reported at core plasma densities exceeding the Greenwald density and neutral beam injection (NBI) power $P_{NBI} \leqslant 0.75$ MW. General

* Corresponding author. Tel.: +1 609 243 2064; fax: +1 609 243 2874.
E-mail address: vlad@llnl.gov (V.A. Soukhanovskii).

0022-3115/$ - see front matter © 2004 Elsevier B.V. All rights reserved.
doi:10.1016/j.jnucmat.2004.10.135

similarities in divertor regimes between MAST and large aspect ratio tokamaks have been observed, except that the detachment would take place at very low target $n_t \simeq 2\text{–}3 \times 10^{18}\ m^{-3}$. This article reports on the first results from divertor regime studies in the National Spherical Torus Experiment (NSTX).

2. Experiment

NSTX is a medium-size low aspect ratio device ($A \geqslant 1.27$, $R = 0.85$ m, $a = 0.67$ m). Long pulse L- and H-mode plasmas ($t \leqslant 1$ s) are a standard operating regime. The analyzed pulse conditions comprised typical $I_p = 0.8\text{–}1.0$ MA, $B_t \leqslant 0.45$ T plasmas heated by 0.8–6 MW neutral beams with $T_e(0) \simeq (0.8\text{–}1.0)$ keV, $\bar{n}_e \simeq (2\text{–}5) \times 10^{19}\ m^{-3}$, $Z_{eff}(0) < 2$, $\tau_E \simeq 50\text{–}100$ ms. A lower single null (LSN) magnetic configuration was utilized with the *drsep* parameter of -1.5 cm (Fig. 1), the ion ∇B drift toward the lower X-point, the elongation of $\kappa = 1.6\text{–}2.2$, triangularity of $\delta = 0.3\text{–}0.4$, $q_{95} \simeq 6\text{–}7$, the X-point height of 15–20 cm, and the flux expansion (evaluated at outer strike point) of 3–4. The plasmas were fueled by injecting deuterium from both a low field side (LFS) injector at about 120 Torr l/s and from a center-stack high field side (HFS) injector at a decreasing rate from 80 to 10 Torr l/s. Whereas this fueling scheme allowed better access to the H-modes, $\bar{n}_e$ increased continuously and non-disruptively [4]. NSTX divertor has an open geometry. The center column, divertor plates, and passive plates are covered with CFC and ATJ graphite tiles 2.5 cm and 5 cm thick. Data from several edge diagnostics shown in Fig. 1 have been used in the present analysis. Experimental divertor physics is inherently two dimensional. Edge and divertor diagnostics in NSTX are point-localized or one dimensional, making the present analysis dependent on the modeling and extrapolation assumptions. Divertor infra-red emissivity profiles are recorded by a 30 Hz infra-red camera, and radial heat flux profiles are inferred using the one dimensional (1D) heat conduction model of the ATJ graphite tiles [5]. Divertor D_α, D_γ and inboard mid-plane D_α brightness profiles are recorded by spectrally filtered 1D CCD arrays [6]. The D_α CCD arrays are photometrically calibrated. The outer mid-plane edge and scrape-off layer (SOL) temperature and density are measured by the Multi-point Thomson scattering system with 2–3 cm spatial resolution. First results from the recently commissioned tile-mounted divertor Langmuir probes and a four chord divertor bolometry system are also used in the analysis.

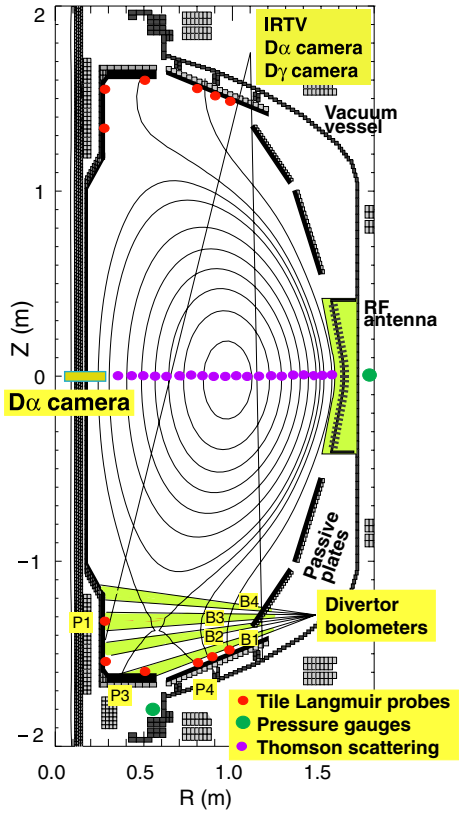

Fig. 1. Schematic of the NSTX cross-section with a lower single null plasma and the diagnostics arrangement.

3. Results and discussion

Despite vast differences in the core and edge power and density operational space of the L- and H-mode LSN plasmas [7,8], one resilient divertor state dominates the operational space. The plasma in the inner divertor is cold and dense, often detached, whereas the outer divertor is always attached. Edge power, recycling, and neutral flux measurements in NSTX have been previously reported [7,9]. We note that the D_α brightness reported in the latter reference must be multiplied by a factor of 51 due to a calibration correction. In general, initial results from the divertor power balance indicate that power accounting in NSTX is fairly good: fast ion losses account for about 20% of the input power, up to 70% reaches the divertor as heat, up to 10% is radiated in the core plasma, up to 10% is radiated in the divertor [10]. Particle balance indicates that the wall is in a pumping state [11], as a result of an effective wall conditioning program on NSTX [12]. To illustrate the observed divertor features, we use an L-mode discharge for which an extended set of diagnostics is available (Fig. 2). A sign of the inner divertor detachment is the increase of the D_γ/D_α brightness ratio. The ratio has been used to identify volume recombination which occurs at $T_e \leqslant 3\text{–}5$ eV and is correlated with an onset of

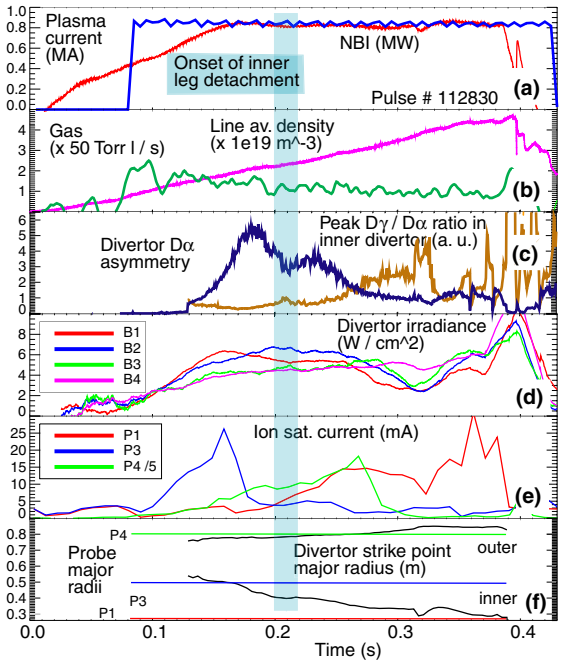

Fig. 2. Time traces of a representative L-mode discharge. (a) Plasma current, input NBI power, (b) line averaged density and gas input, (c) divertor D_γ/D_α ratio and D_α asymmetry parameter A, (d) divertor bolometers, (e) ion saturation currents, (f) strike point major radii from EFIT. Bolometer and probe notations are as in Fig. 1.

detachment [13]. An increase of divertor radiated power is apparent on the two lower chords of the bolometer system B1 and B2. Fig. 3 shows the D_α, D_γ and q_t profiles at the times $t = 0.19$ s and 0.26 s, typical for these plasmas. The inner divertor heat flux being already low gradually decreases beyond the IR camera detectability threshold. The ion saturation current J_{sat} measurements by divertor Langmuir probes (Fig. 2) confirm an uncontrolled drift of the strike points (e.g. P4), and the inner plasma–divertor plate interaction region extending upward (P1). The sharp decrease in J_{sat}, measured by P3 and P4, corresponds to the probe locations crossing plasma separatrix into the private flux zone. Whereas the present data set is somewhat limited in spatial resolution, it is suggestive of the *partial* divertor detachment observed in tokamaks [14].

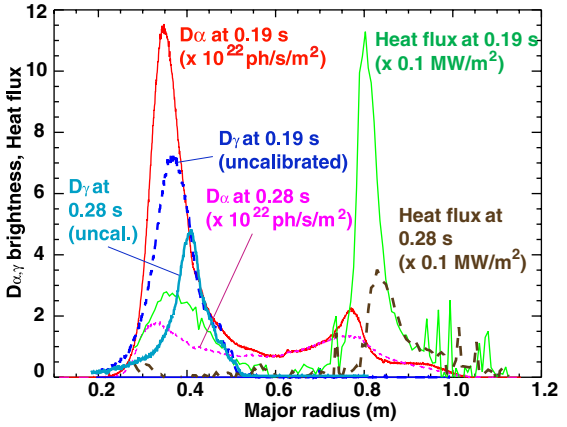

Fig. 3. Divertor D_α, D_γ, and heat flux profiles for the L-mode discharge shown in Fig. 2 at times $t = 0.19$ s and 0.28 s.

We now summarize measured heat flux and recycling trends. Heat fluxes up to 10 MW/m^2 have been measured in NSTX. The peak heat flux increases non-linearly with input power P_{in} in the range 2–6 MW. As in conventional tokamaks higher outboard peak heat fluxes are measured in the L-mode, whereas the inboard heat loads are $q_{in} \leqslant 1$ MW/m^2, being similar in the H- and L-modes, apparently leading to the observed divertor similarities. Inboard and outboard heat fluxes are found to be independent of the the gas fueling location for both the low and high field side gas injectors. This suggests that the NSTX divertor regimes are not affected by the rate of gas puffing $S = 20$–120 Torr s^{-1}. The average inboard power is a factor of 3–5 lower than the outboard, whereas the ratio is about 4–6 for the peak heat flux [7]. Divertor recycling measurements also indicate many similarities in the (P_{in}, n_e) space. The D_α brightness in the inner and outer divertor increases with power in L- and H-mode plasmas. The divertor D_α brightness is almost always higher in L-mode vs H-mode plasmas, although the inner divertor brightness is comparable at $\bar{n}_e \geqslant 3 \times 10^{19}$ m^{-3}. The in–out D_α peak brightness asymmetry develops due to a much faster increase of the inboard emission with $\bar{n}_e$. The asymmetry is 4–6 in the L-mode, and up to 15 in the H-mode plasmas. It is, however, smaller than or about 1 at low densities, and greater than 1 at $\bar{n}_e \simeq 2.5 \times 10^{19}$ m^{-3} in the L-mode, and at slightly higher $\bar{n}_e$ in the H-mode [9]. The asymmetry is always $A \leqslant$ 1–1.5 in ohmic plasmas with $P_{in} \leqslant 0.7$ MW. The asymmetry in recycling has been observed in large aspect ratio tokamaks, and in many cases is attributed to the inner divertor detachment, in some instances accompanied by an X-point MARFE [15,16]. Several factors, which can be at play simultaneously, may contribute to the development of the D_α emission asymmetry: the temperature and density dependence of atomic rates [13], different inner and outer flux tube lengths [17], and the radial $E \times B$ drift [18]. The latter can be substantial in the recycling (high density) regime, resulting in a high drift velocity directed toward the inner target for ∇B toward the lower X-point. In NSTX a large asymmetry ($A > 2$) often correlates with the increase of the D_γ/D_α ratio. The measured D_α brightness in the inner and outer divertor is consistent with emissivity estimates obtained from the calculated deuterium Balmer α emissivity rates [13] for $T_e \simeq 2$–5 eV, $n_e \leqslant 10^{20}$ m^{-3} recombining plasmas and $T_e \simeq 10$–30 eV,

$n_e \leqslant 5 \times 10^{19}$ m^{-3} ionizing plasmas, suggestive of inner divertor detachment. Another supporting factor for this notion is the lower divertor recycling behavior in the ELMy H-mode plasmas. The divertor state is resilient to the impact of ELMs. H-mode plasma regimes with type I, type III, and type V ELMs have been identified in NSTX [19]. When the type I and III ELMs ($0.01 < \Delta W/W < 0.30$, where W is the plasma stored energy) reach the lower divertor the recycling profile asymmetry transiently reverses ($A < 1$), and recovers between ELMs (Fig. 4), suggestive of a transient re-attachment of the detached inner divertor as the heat flux is transiently increased during the ELM heat pulse. Similar recycling behavior has been reported in large aspect ratio tokamaks [15,20].

Since direct T_e, n_e divertor measurements are not yet available in NSTX, the two point model (2PM) of the scrape-off layer (SOL) transport [1] is used to estimate plasma conditions in the divertor. The 2PM relates the plasma parameters at the divertor target T_t, n_t, Γ_t to the 'upstream' parameters through the Spitzer heat conduction equation, the pressure balance in a flux tube, and the sheath condition at the target surface [1]. The 2PM does not include any radiation effects and any ST relevant factors. The measured outer mid-plane SOL $T_e^{sep} \simeq 20$–40 eV and $n_e^{sep} \simeq 2$–7×10^{18} m^{-3} yield a SOL collisionality $\nu_e^* \geqslant 10$, suggesting that the outer divertor is either in the sheath-limited or high recycling regime. The 2PM predicts $T_t^{out} \leqslant 30$ eV, $n_t^{out} \leqslant 7 \times 10^{18}$ m^{-3} for the outer divertor if the measured heat flux density $q_{in} \leqslant 6$ MW/m^2 and the connection length of $L_c \simeq 30$ m are used. For inner divertor parameters $q_{in} \leqslant 1$ MW/m^2, $L_c \leqslant 30$ m this estimate yields $T_t^{in} \simeq 1$–7 eV, $n_t^{in} \leqslant 8 \times 10^{19}$ m^{-3}. The estimates suggest that the inner target plasma is cold and dense, and may be detached, whereas the outer target operates in the sheath-limited and flux limited (high-recycling) regimes. The non-linear dependence of the peak D_α brightness on density and divertor D_α in-out asymmetry also support this notion, as $n_t \sim n_u^3$, $T_t \sim n_u^{-2}$ in the high-recycling regime, whereas T_t decreases and n_t increases as the detachment occurs, leading to the observed increase in D_α intensity. Efforts to use the multi-fluid code UEDGE with purely diffusive and diffusive–convective models for the divertor analysis have had moderate success: the modeling has not been able to accurately reproduce the observed D_α asymmetry, and match the edge T_e, n_e profiles and divertor heat fluxes [21,22]. Nevertheless, the modeling is very useful in guiding experimental work. An example of this is shown in Fig. 5: UEDGE with an anomalous diffusive radial transport model is used to estimate the detachment boundaries [21,23]. Input power and electron density at the core boundary ($\psi_N = 0.9$) are systematically varied using an H-mode LSN equilibrium and measured edge profiles. The model includes carbon impurities with the source determined by physical and chemical sputtering from all plasma facing surfaces. Two criteria for divertor detachment are used: the decrease of peak divertor T_e to 5 eV or less, and the saturation of the total ion current to the plate as the upstream density is increased. The two criteria have led to similar results and correctly predicted the onset of the detachment. However, the observed detachment boundaries are much wider, the inner divertor is attached in ohmic ($P_{in} \leqslant 0.7$ MW) and low density plasmas, and the outer divertor detachment has not been observed even in plasmas with $n_e(\psi_{90}) \leqslant 6 \times 10^{19}$ m^{-3}. In summary, initial analysis of NSTX divertor operation suggests that due to a strong heat flux dispersal in the inner divertor in the L- and H-mode plasmas ($q_t \leqslant 1$ MW/m^2) the inner divertor operates in a detached state at $\bar{n}_e \geqslant 2$–$3\times\ 10^{19}$ m^{-3} ($0.2 \leqslant \bar{n}_e/n_G \leqslant 0.9$), $P_{in} = 1.5$–7 MW, whereas the outer

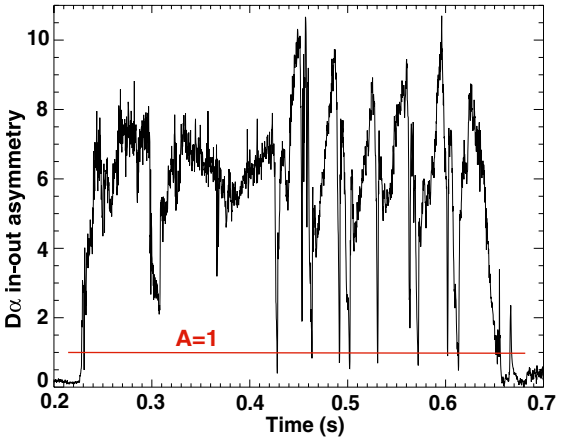

Fig. 4. Example of the reversal of the divertor recycling in-out asymmetry in a double null ELMy H-mode plasma. Transient asymmetry drops ($A \leqslant 1$) occur when ELMs reach the divertor and the inner divertor leg re-attaches.

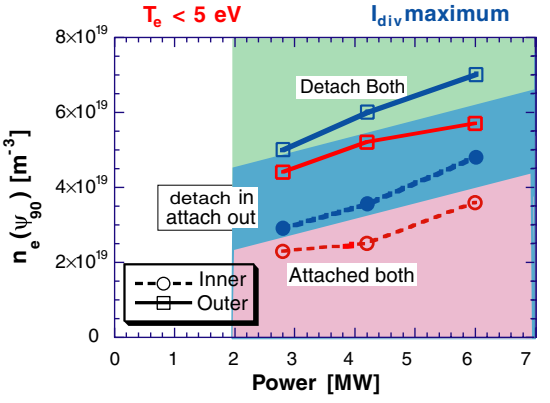

Fig. 5. Divertor detachment mapping in the ($P_{in} - n_e$) space predicted by UEDGE using the $T_e \leqslant 5$ eV and I_{sat} criteria (red and blue lines).

divertor is always attached. Future experiments will explore the divertor operational space further, attempting to produce a fully detached radiative divertor by increasing the core density and edge radiated power, and studying the role of impurities and electromagnetic drifts in the detachment process.

Acknowledgements

The authors thank D. Gates, D. Mueller, and T. Stevenson (PPPL) for operating the NSTX device, and S. Sabbagh (Columbia University) for EFIT magnetic equilibrium reconstructions. This research was supported by the US Department of Energy under contracts No. W-7405-Eng-48, DE-AC02-76CH03073, DE-AC05-00OR22725.

References

[1] P.C. Stangeby, The plasma boundary of Magnetic Fusion Devices, IoP, Bristol and Philadelphia, 2000.
[2] A. Kirk, W. Fundamenski, J.-W. Ahn, G. Counsell, Plasma Phys. Control. Fus. 45 (8) (2003) 1445.
[3] G. Counsell, J.-W. Ahn, R. Cohen, A. Kirk, P. Helander, R. Martin, D. Ryutov, A. Tabasso, H. Wilson, Y. Yang, the MAST Team, Nucl. Fus. 43 (10) (2003) 1197.
[4] R. Maingi, C.S. Chang, S. Ku, T. Biewer, R. Maqueda, M. Bell, R. Bell, C. Bush, D. Gates, S. Kaye, H. Kugel, B. LeBlanc, J. Menard, D. Mueller, R. Raman, S. Sabbagh, V. Soukhanovskii, the NSTX Team, Plasma Phys. Control. Fus. 46 (5A) (2004) A305.
[5] R. Maingi, H.W. Kugel, C.J. Lasnier, A.L. Roquemore, V.A. Soukhanovskii, C.E. Bush, J. Nucl. Mater. 313 (2003) 1005.
[6] V.A. Soukhanovskii, A.L. Roquemore, C.H. Skinner, D. Johnson, R. Maingi, C. Bush, F. Paoletti, S. Sabbagh, Rev. Sci. Instrum. 74 (2003) 2094.
[7] R. Maingi, M. Bell, R. Bell, C. Bush, E. Fredrickson, D. Gates, T. Gray, D. Johnson, R. Kaita, S. Kaye, S. Kubota, H. Kugel, C. Lasnier, B. LeBlanc, R. Maqueda, D. Mastrovito, J. Menard, D. Mueller, M. Ono, F. Paoletti, S. Paul, Y.-K. Peng, A. Roquemore, S. Sabbagh, C. Skinner, V. Soukhanovskii, D. Stutman, D. Swain, E. Synakowski, T. Tan, J. Wilgen, S. Zweben, Nucl. Fus. 43 (9) (2003) 969.
[8] R. Maingi, M.G. Bell, R.E. Bell, J. Bialek, C. Bourdelle, C.E. Bush, D.S. Darrow, E.D. Fredrickson, D.A. Gates, M. Gilmore, T. Gray, T.R. Jarboe, D.W. Johnson, R. Kaita, S.M. Kaye, S. Kubota, H.W. Kugel, B.P. LeBlanc, R.J. Maqueda, D. Mastrovito, S.S. Medley, J.E. Menard D. Mueller, B.A. Nelson, M. Ono, F. Paoletti, H.K. Park, S.F. Paul, T. Peebles, Y.-K.M. Peng, C.K. Phillips, R. Raman, A.L. Rosenberg, A.L. Roquemore, P.M. Ryan, S.A. Sabbagh, C.H. Skinner, V.A. Soukhanovskii, D. Stutman, D.W. Swain, E.J. Synakowski, G. Taylor, J. Wilgen, J.R. Wilson, G.A. Wurden, S.J. Zweben, the NSTX Team, Plasma Phys. Control. Fus. 45 (5) (2003) 657.
[9] V.A. Soukhanovskii, R. Maingi, R. Raman, H.W. Kugel, B.P. LeBlanc, A.L. Roquemore, C. Lasnier, in: R. Koch, S. Lebedev (Eds.), Proceedings of the 30th EPS Conference on Plasma Physics and Controlled Fusion, St. Petersburg, Russia, 2003.
[10] S. Paul et al., these Proceedings.
[11] V.A. Soukhanovskii, R. Maingi, R. Raman, H.W. Kugel, B.P. LeBlanc, A.L. Roquemore, C.H. Skinner, J. Nucl. Mater. 313 (2003) 573.
[12] H.W. Kugel, V.A. Soukhanovskii, M. Bell, W. Blanchard, D. Gates, B. LeBlanc, R. Maingi, D. Muller, H.K. Na, S. Paul, C.H. Skinner, D. Stutman, W.R. Wampler, J. Nucl. Mater. 313–316 (2003) 187.
[13] G.M. McCracken, M.F. Stamp, R.D. Monk, A.G. Meigs, J. Lingertat, R. Prentice, A. Starling, R.J. Smith, A. Tabasso, Nucl. Fus. 38 (4) (1998) 619.
[14] T. Petrie, D. Hill, S. Allen, N. Brooks, D. Buchenauer, J. Cuthbertson, T. Evans, P. Ghendrih, C. Lasnier, A. Leonard, R. Maingi, G. Porter, D. Whyte, R. Groebner, R. Jong, M. Mahdavi, S. Thompson, W. West, R. Wood, Nucl. Fus. 37 (3) (1997) 321.
[15] A. Loarte, R. Monk, J. Martín-Solís, D. Campbell, A. Chankin, S. Clement, S. Davies, J. Ehrenberg, S. Erents, H. Guo, P. Harbour, L. Horton, L. Ingesson, H. Jäckel, J. Lingertat, C. Lowry, C. Maggi, G. Matthews, K. McCormick, D. O'Brien, R. Reichle, G. Saibene, R. Smith, M. Stamp, D. Stork, G. Vlases, Nucl. Fus. 38 (3) (1998) 331.
[16] A. Hatayama, H. Segawa, N. Komatsu, R. Schneider, D.P. Coster, N. hayashi, S. sakurai, N. Asakura, J. Nucl. Mater. 290–293 (2001) 407.
[17] U. Wenzel, D. Coster, A. Kallenbach, H. Kastelewicz, M. Laux, H. Maier, R. Schneider, AU Team, Nucl. Fus. 41 (11) (2001) 1695.
[18] P. Stangeby, A. Chankin, Nucl. Fus. 36 (7) (1996) 839.
[19] R. Maingi et al., these Proceedings. doi:10.1016/j.jnucmat.2004.08.023.
[20] M. Groth, M.E. Fenstermacher, J.A. Boedo, N.H. Brooks, D.S. Gray, C.J. Lasnier, A.W. Leonard, G.D. Porter, J.G. Watkins, J. Nucl. Mater. 313–316 (2003) 1071.
[21] M.E. Rensink, H.W. Kugel, R. Maingi, F. Paoletti, G.D. Porter, T.D. Ronglien, S. Sabbagh, X. Xu, J. Nucl. Mater. 290–293 (2001) 706.
[22] A.Yu. Pigarov (UCSD) and G.D. Porter (LLNL), Personal communication.
[23] N.S. Wolf, G.D. Poter, D.N. Hill, S.L. Allen, J. Nucl. Mater. 266–269 (1999) 739.